



Article

Al-Doped Octahedral Cu₂O Nanocrystal for Electrocatalytic CO₂ Reduction to Produce Ethylene

Sanxiu Li [†], Xuelan Sha [†], Xiafei Gao and Juan Peng ^{*†}

State Key Laboratory of High-Efficiency Utilization of Coal and Green Chemical Engineering, College of Chemistry and Chemical Engineering, Ningxia University, Yinchuan 750021, China; sanxiu2023@163.com (S.L.); shaxuelan2023@163.com (X.S.); gaomiaofei0204@163.com (X.G.)

* Correspondence: pengjuan@nxu.edu.cn

[†] These authors contributed equally to this work.

Abstract: Ethylene is an ideal CO₂ product in an electrocatalytic CO₂ reduction reaction (CO₂RR) with high economic value. This paper synthesised Al-doped octahedral Cu₂O (Al–Cu₂O) nanocrystal by a simple wet chemical method. The selectivity of CO₂RR products was improved by doping Al onto the surface of octahedral Cu₂O. The Al–Cu₂O was used as an efficient electrocatalyst for CO₂RR with selective ethylene production. The Al–Cu₂O exhibited a high % Faradaic efficiency (FE_{C₂H₄}) of 44.9% at –1.23 V (vs. RHE) in CO₂ saturated 0.1 M KHCO₃ electrolyte. Charge transfer from the Al atom to the Cu atom occurs after Al doping in Cu₂O, optimizing the electronic structure and facilitating CO₂RR to ethylene production. The DFT calculation showed that the Al–Cu₂O catalyst could effectively reduce the adsorption energy of the *CHCOH intermediate and promote the mass transfer of charges, thus improving the FE_{C₂H₄}. After Al doping into Cu₂O, the center of d orbitals shift positively, which makes the d-band closer to the Fermi level. Furthermore, the density of electronic states increases due to the interaction between Cu atoms and intermediates, thus accelerating the electrochemical CO₂ reduction process. This work proved that the metal doping strategy can effectively improve the catalytic properties of Cu₂O, thus providing a useful way for CO₂ cycling and green production of C₂H₄.

Keywords: electrocatalysis; electronic structure; faradaic efficiency; ethylene



Citation: Li, S.; Sha, X.; Gao, X.; Peng, J. Al-Doped Octahedral Cu₂O Nanocrystal for Electrocatalytic CO₂ Reduction to Produce Ethylene. *Int. J. Mol. Sci.* **2023**, *24*, 12680. <https://doi.org/10.3390/ijms241612680>

Academic Editor: Ilya Nifant'ev

Received: 9 July 2023

Revised: 4 August 2023

Accepted: 8 August 2023

Published: 11 August 2023



Copyright: © 2023 by the authors. Licensee MDPI, Basel, Switzerland. This article is an open access article distributed under the terms and conditions of the Creative Commons Attribution (CC BY) license (<https://creativecommons.org/licenses/by/4.0/>).

1. Introduction

The increased CO₂ emissions in the atmosphere result in a serious greenhouse effect and the elevated sea level [1,2]. The electrochemical CO₂ reduction reaction (CO₂RR) is a promising strategy to mitigate the global warming and energy crisis while transforming CO₂ into fuels and chemical feedstocks [3–5]. It can use clean electric energy generated by renewable solar and wind energy to drive the conversion of CO₂ under mild conditions [6,7]. Electroreduction of CO₂ in molten salts, also called molten salt carbon capture and electrochemical transformation (MSCC-ET), is an advanced method which can capture carbon dioxide from the atmosphere or flue gases [8–11]. The reduction products of CO₂RR include CO [12–14], HCOOH [15–18], alcohols [19–21], and various hydrocarbons [22–24]. Among them, C₂H₄ has attracted more and more attention due to its high energy density. Furthermore, C₂H₄ is essential in producing various plastics, solvents, and cosmetics in the chemical industry [25].

Up to now, Cu-based materials can electrocatalytic convert CO₂ into C₂/C₂+ products. Among reported Cu-based catalysts, Cu₂O nanocrystal has attracted much attention due to their electrocatalytic activity and high selectivity toward C₂H₄. To improve the CO₂RR performance of Cu₂O, great efforts have been made on its structural design. Metal ions can be used as structure-guiding agents to optimize the micro-structure of nanocrystals [26]. Cu₂O nanoparticles (Cu₂O NPs) exhibit good performance for CO₂RR, possibly because

the low coordination Cu^+ on the surface contributes to C-C coupling, thus promoting the production of C_2H_4 [27]. Other strategies, including crystal facet controlling [28], defect engineering [29,30], alloying [31], valence adjustment [32], and surface molecular modification [24], have been employed to improve the electrocatalytic performance of CO_2RR to produce C_2H_4 . For example, Shang et al. [33] have designed a core-shell $\text{Cu@Cu}_2\text{O}$ catalyst on which a thin layer of natural oxide grows on the surface under environmental conditions. The synergistic effect between Cu^+ and Cu^0 on the $\text{Cu@Cu}_2\text{O}$ surface helps to improve its efficiency and selectivity for C2 products. Ning et al. [34] reported the preparation of Cu_2O /nitrogen-doped carbon shell ($\text{Cu}_2\text{O}/\text{NCS}$) composite and its application in CO_2 electroreduction to selective formation of C_2H_4 . However, copper-based catalysts still face many problems, such as inevitable competitive hydrogen evolution reaction (HER), complex reaction mechanisms diversification of products, and low selectivity of target products [35]. Therefore, it is of huge challenge to design CO_2RR electrocatalysts with high activity, selectivity, and satisfied stability.

This work proposed an effective strategy to improve the CO_2RR activity by doping Al on the surface of octahedron Cu_2O nanocrystals. Al-doped Cu_2O ($\text{Al-Cu}_2\text{O}$) was used as an effective electrocatalyst for selective ethylene production by CO_2RR . $\text{Al-Cu}_2\text{O}$ exhibits a high Faraday efficiency ($\text{FE}_{\text{C}_2\text{H}_4}$) of 44.9% at -1.23 V (vs. RHE). During the coupling process of $^*\text{CHCOH}$ intermediate, the $\text{Al-Cu}_2\text{O}$ catalyst can significantly reduce the free energy and promote the formation of C_2H_4 . It can also inhibit the occurrence of HER side reaction. Therefore, the doping strategy is beneficial for the adsorption of intermediates to reconstruct the internal stable state of Cu_2O , thus improving the activity and selectivity of CO_2 conversion to ethylene.

2. Results and Discussion

2.1. Morphology and Structure Analysis

As shown in Figure 1, $\text{Al-Cu}_2\text{O-X}$ nanocrystals were prepared by a simple one-step method (Experimental section for details). To further characterize $\text{Al-Cu}_2\text{O-X}$ catalysts, the XRD pattern was used to study Cu_2O , $\text{Al-Cu}_2\text{O}$, and $\text{Al-Cu}_2\text{O-2}$ crystal structure. From the XRD pattern in Figure 2a, the peaks at 29° , 36° , 42° , 61° , 73° , and 77° correspond to the (110), (111), (200), (220), (311), and (222) planes of Cu_2O , respectively, which agree well with the octahedral Cu_2O (PDF#75-1535). The XRD patterns of $\text{Al-Cu}_2\text{O-X}$ (3-6) are shown in Figure S1. During the preparation process, the catalyst was synthesized by adjusting the amount of Al^{3+} , the concentration of NaOH, and the reaction time. $\text{Al-Cu}_2\text{O-X}$ (3-6) were all single-phase Cu_2O nanocrystals. The morphologies of the Cu_2O , $\text{Al-Cu}_2\text{O}$, and $\text{Al-Cu}_2\text{O-2}$ were monitored by scanning electron microscopy (SEM). Cu_2O nanocrystals without Al doping showed an octahedron shape with a smooth surface (Figure S2a). Due to the doping effect of Al, the $\text{Al-Cu}_2\text{O}$ nanocrystal presented an octahedral shape with a more rough surface and formed a defect structure (Figure 2b), which may provide abundant active sites for CO_2RR [36]. When the concentration of Al^{3+} increased from 0.02 M to 0.03 M, $\text{Al-Cu}_2\text{O-2}$ catalyst exhibits a cube shape (Figure S2b). However, it was reported that the resulting cube $\text{Al-Cu}_2\text{O}$ catalyst is not conducive to forming C_2H_4 [27]. The better-performing $\text{Al-Cu}_2\text{O}$ with a homo-octahedral shape was observed by TEM (Figure 2c), which was consistent with the SEM image. The high-resolution transmission electron microscopy (HRTEM) image in Figure 2d presented that the lattice stripe spacing d marked was 0.304 nm, corresponding to the (110) crystal plane of Cu_2O . The HAADF-STEM image (Figure 2e) also exhibited an octahedral shape. The composition of $\text{Al-Cu}_2\text{O}$ was reconfirmed by elemental mapping (Figure 2f). The Al (red), Cu (blue), and O (green) elements are uniformly distributed over the $\text{Al-Cu}_2\text{O}$ nanocrystals.

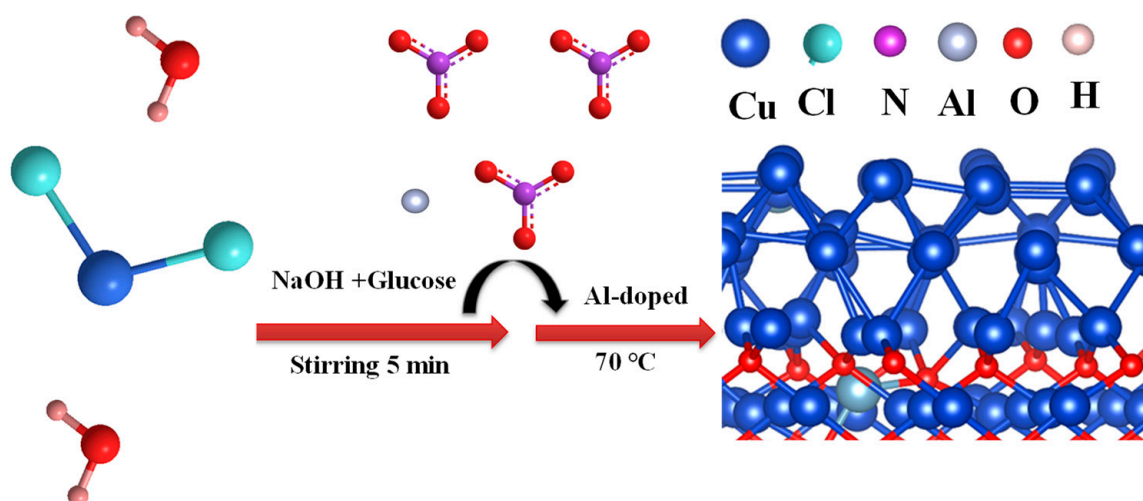


Figure 1. Schematic illustration of the fabrication process for Al-Cu₂O-X (X = 2, 3, 4, 5, 6).

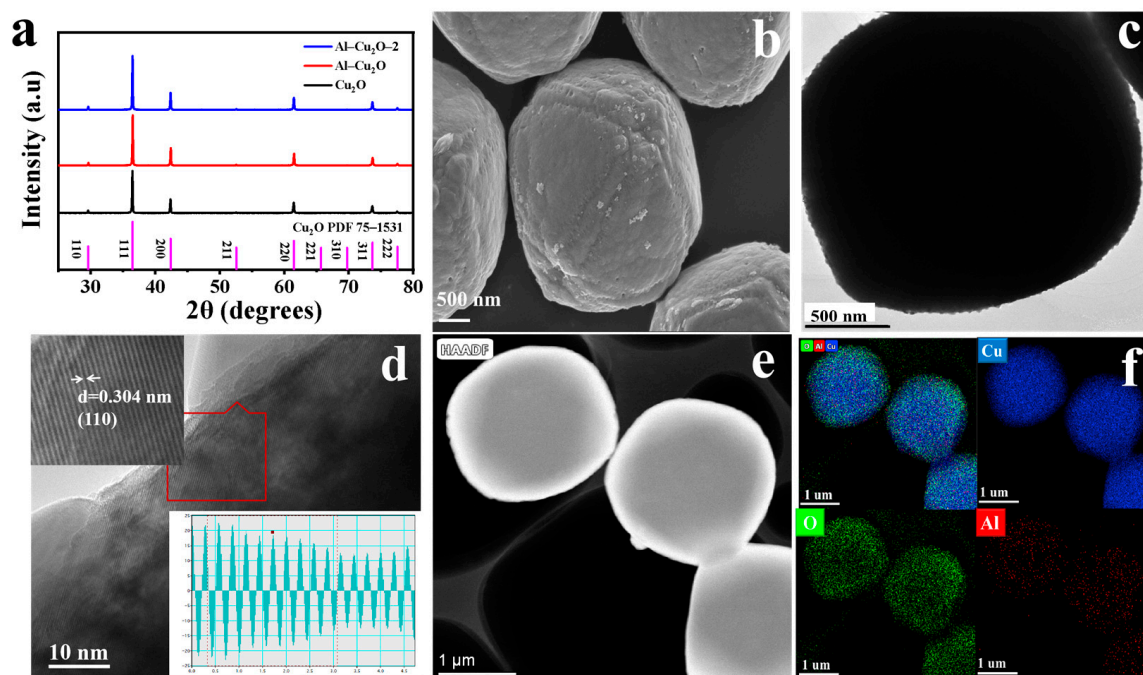


Figure 2. Characterization of Al-Cu₂O: (a) XRD, (b) SEM, (c) TEM, (d) HRTEM, (e) HAADF-TEM, and (f) elemental mapping (blue, green and red represents Cu, O and Al element, respectively).

The surface composition and valence of Cu₂O and Al-Cu₂O nanocrystals were characterized by X-ray photoelectron spectroscopy (XPS). As shown in Figure 3a,b, four peaks were observed in Cu 2p spectrum for both Cu₂O and Al-Cu₂O samples. For Cu₂O, the peaks at 932.78 and 952.62 eV corresponded to the binding energies of Cu 2p_{3/2} and Cu 2p_{1/2} of Cu₂O or Cu, respectively. The binding energies at 935.28 eV and 944.48 eV were ascribed to the peaks of Cu²⁺. For Al-Cu₂O, the 932.89 and 952.73 eV peaks corresponded to the Cu 2p_{3/2} and Cu 2p_{1/2} of Cu₂O or Cu, respectively. The binding energy of 935.26 and 944.46 eV belonged to the peak of Cu²⁺. The above results showed that the existence of Cu⁰ may be due to the partial reduction of Cu₂O in the CO₂RR process [37]. The existence of trace CuO may be mainly due to the oxidation of a small amount of Cu₂O catalyst to CuO in the air after the synthesis of Cu₂O [38]. When octahedral Cu₂O nanocrystals were doped with Al, the peaks of Cu 2p_{3/2}, Cu 2p_{1/2}, and Cu²⁺ of Cu₂O or Cu were shifted positively. These results may be attributed to the introduction of Al, which can induce charge transfer from Al atoms to Cu atoms, thus modulating the electronic structure

of Al-Cu₂O. The existence of Cu₂O was also confirmed in the O 1s XPS spectra of Cu₂O and Al-Cu₂O (Figure 3c,d). There were three XPS peaks in both catalysts, of which the peak at 530.5 eV corresponded to the Cu-O bond, and 532.11 and 532.77 eV corresponded to O_{lat} and C=O, respectively [39]. In the high-resolution spectrum of Al 2p (Figure 3e), the peaks at 74.55 and 77.35 eV corresponded to the Al 2p_{1/2} and Al 2p_{3/2} of metal Al, respectively. The Al atom was 0.41% by XPS analysis, indicating that the Al-Cu₂O catalyst has been successfully prepared.

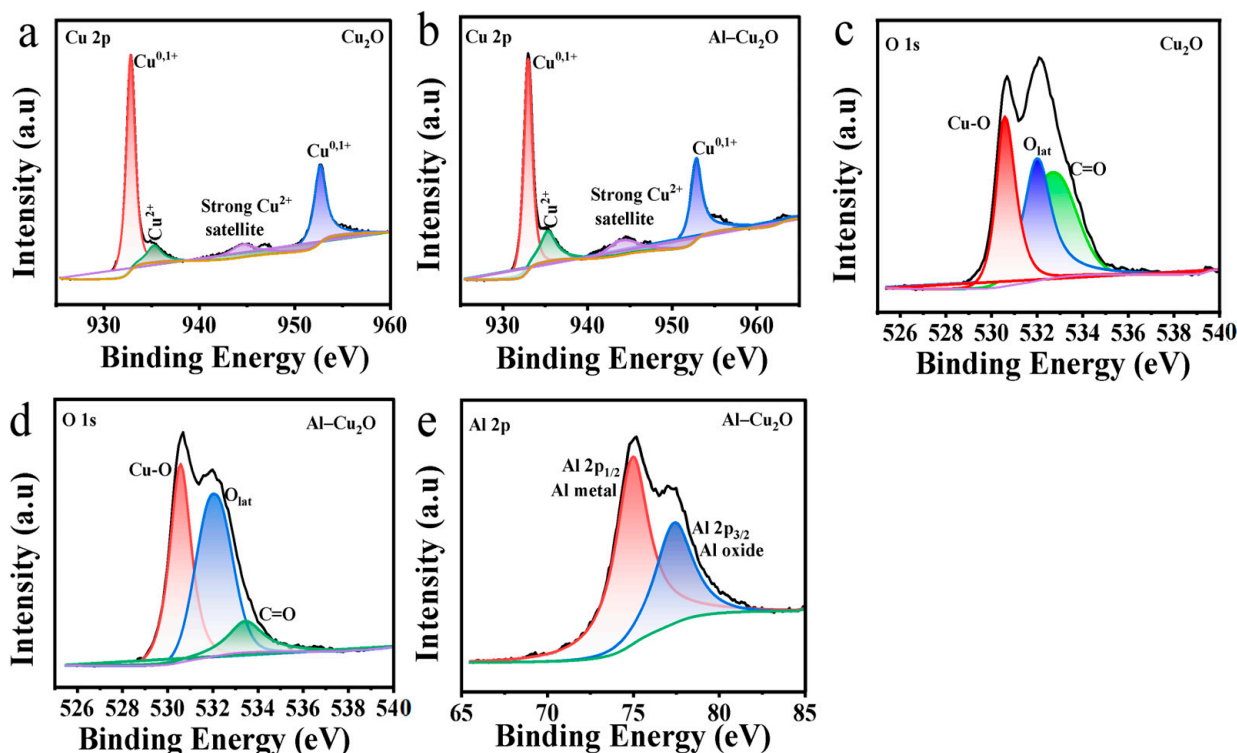


Figure 3. XPS spectrum of Cu 2p: (a) Cu₂O and (b) Al-Cu₂O; O 1s spectrum of (c) Cu₂O and (d) Al-Cu₂O, (e) Al 2p spectrum of the Al-Cu₂O.

2.2. Electrocatalytic CO₂RR Performances

To further analyze the electrochemical performance of the catalyst, the linear sweep voltammetry (LSV) of Cu₂O and Al-Cu₂O-X in saturated CO₂ electrolyte and saturated N₂ electrolyte were tested. The analysis of Figure 4a shows that the current density of Al-Cu₂O catalyst in CO₂ saturated electrolyte is higher than that in N₂, indicating that Al-Cu₂O catalyst had higher activity to CO₂RR. The LSV curve was measured in a CO₂-saturated 0.1 M KHCO₃ electrolyte (Figure S3a). The current density of the Al-Cu₂O catalyst in CO₂ saturated electrolyte was higher than that of Cu₂O and Al-Cu₂O-2 catalysts, indicating that the Al-Cu₂O catalyst had better electrocatalytic activity to CO₂RR. Figure S3b shows the potentiostatic electrolysis of CO₂ at various potentials. The almost constant current signal indicated that the Al-Cu₂O catalyst exhibited good electrochemical stability during the CO₂RR process. In Figure 4b, the formation rates of three kinds of catalysts were presented for ethylene products. The Al-Cu₂O catalyst had a higher current density for ethylene formation than that of Cu₂O and the Al-Cu₂O-2 catalysts in a wide potential range. The partial current density of 16.7 mA cm⁻² was achieved at -1.38 V (vs. RHE). The above results showed that the Al-Cu₂O catalyst was more conducive to producing ethylene as the main product and has a better inhibitory effect on competition for hydrogen formation.

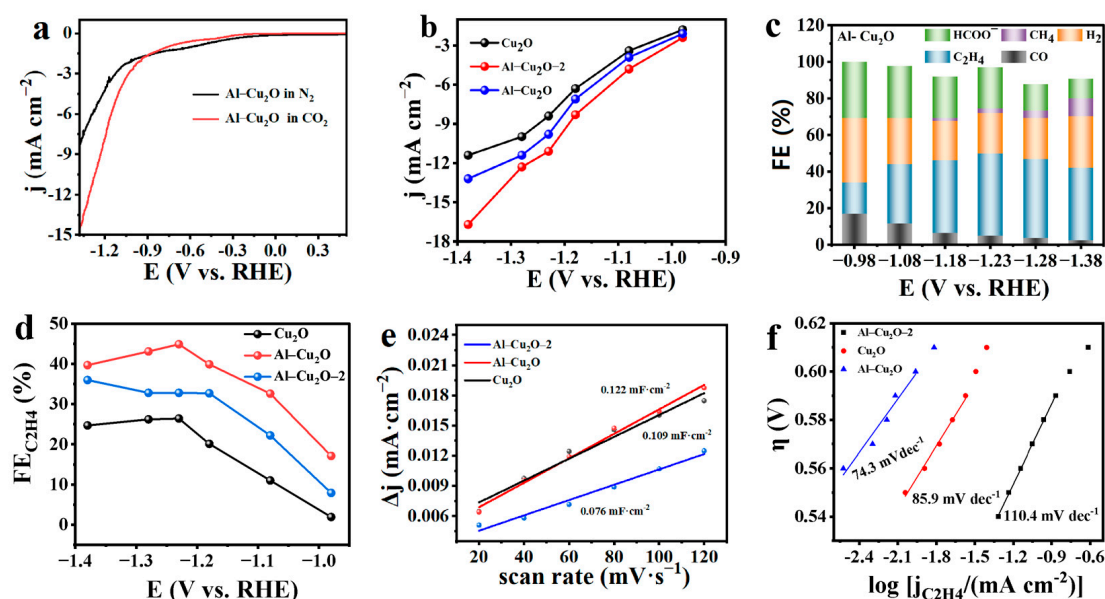


Figure 4. (a) LSV curves of Cu_2O , $\text{Al-Cu}_2\text{O}$ and $\text{Al-Cu}_2\text{O-2}$ catalysts in 0.1 M KHCO_3 aqueous solutions saturated CO_2 , (b) partial current density of Cu_2O , $\text{Al-Cu}_2\text{O}$ and $\text{Al-Cu}_2\text{O-2}$ catalysts, sweeping speed of 5 mV s^{-1} , (c) FE values of $\text{Al-Cu}_2\text{O}$ catalyst in 0.1 M KHCO_3 aqueous solutions with saturated CO_2 , (d) The $\text{FE}_{\text{C}_2\text{H}_4}$ values of Cu_2O , $\text{Al-Cu}_2\text{O}$ and $\text{Al-Cu}_2\text{O-2}$ catalysts, (e) The linear relationship between Δj and scanning rates, (f) Tafel plots of Cu_2O , $\text{Al-Cu}_2\text{O}$ and $\text{Al-Cu}_2\text{O-2}$.

To determine the CO_2RR selectivity of the $\text{Al-Cu}_2\text{O}$ catalyst, the reduction products were qualitatively and quantitatively analyzed. In this study, the reduction products of each catalyst were determined in the wide potential range from -0.98 V to -1.38 V (vs. RHE). From Figures 4c and 5, the CO_2RR products by Cu_2O , and $\text{Al-Cu}_2\text{O-X}$ catalysts were C_2H_4 , HCOO^- , CO , CH_4 and by-product H_2 . Figure 5a shows the FE of the electrochemical CO_2RR product catalyzed by an octahedral Cu_2O nanocrystal catalyst without the Al doping. The octahedral Cu_2O nanocrystal catalyst had a good effect on inhibiting HER at low potential, and the $\text{FE}_{\text{C}_2\text{H}_4}$ was 26.1%. As shown in Figure 4b, with the potential increase, the FE value of H_2 decreases from 35.1% to 22.1%.

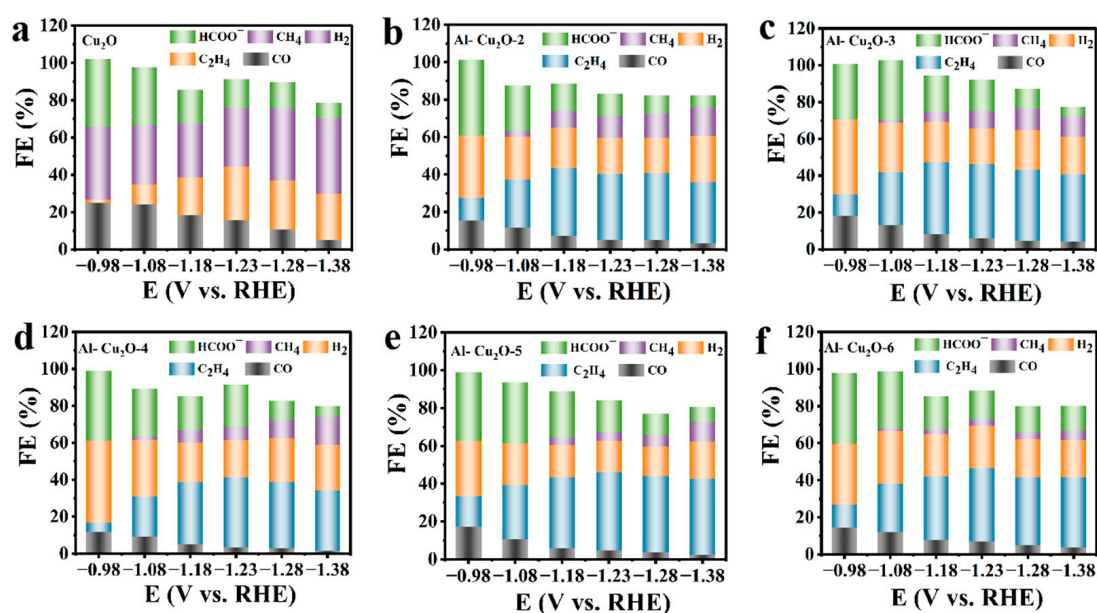


Figure 5. (a–f) FE values of Cu_2O and $\text{Al-Cu}_2\text{O-X}$ ($X=2, 3, 4, 5, 6$) catalysts in 0.1 M KHCO_3 aqueous solutions with saturated gas CO_2 .

On the contrary, the FE value of C_2H_4 increases to 44.9% at -1.23 V (vs. RHE). The results showed the catalyst's good selectivity for ethylene production and inhibition effect on HER. If an appropriate amount of Al (0.02 M) was introduced into the octahedral Cu_2O nanocrystal (Figure 4c), the selectivity of the Al- Cu_2O catalyst was improved. If more Al^{3+} was added to the reaction, the result showed that the FE of C_2H_4 was 32.8%, indicating that the catalyst had a good selectivity for ethylene (Figure 5b). We also studied the effects of catalysts synthetic conditions, including reaction time (Figure 5c,d) and NaOH concentration (Figure 5e,f), on the selectivity of the CO_2RR product. The results indicated that optimising reaction time and NaOH concentration could give the catalyst a certain selectivity. Figure 4d compares the selectivity of three kinds of catalysts (Cu_2O , Al- Cu_2O , and Al- Cu_2O-2) for ethylene products. Under different applied potentials, the efficiency of the Al- Cu_2O catalyst for CO_2RR to C_2H_4 was higher than that of the other two catalysts. This result suggested that the Al introduced into the catalyst affected the selectivity of the catalyst. This may be because Al-doped Cu_2O will cause changes in the electronic structure and the morphology of the catalyst, thus reducing the adsorption energy of the catalyst for ethylene intermediates in the CO_2RR process and enhancing the selectivity of the reaction to the products. It was worth noting that the Faradaic efficiencies sometimes do not reach 100%. A small number of liquid products may still be produced in the electrocatalysis process.

The electrochemical surface area (ECSA) is also a key point for the electrocatalyst. According to the formula for calculating ECSA, it is known that this parameter is related to the C_{dl} and C_{ds} values of their catalysts because the catalysts are coated on hydrophobic carbon paper (model 060). Therefore, the C_{ds} of the three catalysts are the same, and only the C_{dl} value of the catalyst can be calculated to determine the ECSA of the catalyst. According to the cyclic voltammograms (Figure S4a–c) of Cu_2O , Al- Cu_2O , and Al- Cu_2O-2 catalysts at different scanning rates (20, 40, 60, 80, 100, 120 $mV s^{-1}$), the capacitance values of Cu_2O , Al- Cu_2O , and Al- Cu_2O-2 catalysts were 0.109, 0.122, and 0.076 $mF cm^{-2}$, respectively, as shown in Figure 4e. The largest C_{dl} of the Al- Cu_2O electrocatalyst suggested the high electrochemical activity surface area of the Al- Cu_2O-2 catalyst. This high ECSA can offer a lot of catalytic active sites for improving the electrocatalytic performance of CO_2RR , which was consistent with the previous research conclusion.

The impedance of Cu_2O and Al- Cu_2O catalysts under open-circuit voltage was obtained (Figure S5). The EIS arc of the Al- Cu_2O catalyst was smaller than that of the Cu_2O catalyst. The results indicate that interface charges can be rapidly transferred during the reaction process, and catalytic activity can be improved. To better understand the activity and kinetics of Al- Cu_2O materials on CO_2RR , the Tafel slope analysis of the local current density of the catalyst product was carried out. As shown in Figure 4f, the Tafel slope of the Al- Cu_2O catalyst (74.3 $mV dec^{-1}$) was lower than that of Cu_2O (85.9 $mV dec^{-1}$) and the Al- Cu_2O-2 (110.4 $mV dec^{-1}$), indicating that the electron transfer rate of the catalyst is faster, which was beneficial to the rapid adsorption and desorption of the important intermediate from the surface of Al- Cu_2O catalyst.

The stability of the Al- Cu_2O catalyst was investigated in the CO_2RR process. As seen in Figure 6a, the current density of the Al- Cu_2O catalyst can be kept stable, and the FE of ethylene can be kept above 40% in the first 3600 s. With the change in reaction time, the current density increases gradually. However, the selectivity of the catalyst to ethylene decreased obviously after two hours of electrolysis. This may be because of the shedding of the catalyst in the long-term electrolysis process, resulting in a decrease in the FE of the catalyst. The stability of copper-based catalysts is poor. Therefore, other strategies must be used to improve the stability of copper-based catalysts for a long time [40]. The XRD pattern after long-term electrolysis showed that the Al- Cu_2O showed good structure stability (Figure 6b) in the whole CO_2RR test. After the electrolysis of the Al- Cu_2O catalyst for 10 min, 20 min, 30 min and 7 h (Figure S6a–d), the morphology of the octahedron remains unchanged. With the increase of electrolysis time, some small pores appear on the catalyst's surface. The appearance of these pores may provide more active sites, resulting

in an increase in current density in the electrolysis process. However, it yielded a decrease in the FE of ethylene. The above results show that the catalyst can maintain stability under long-term electrolysis.

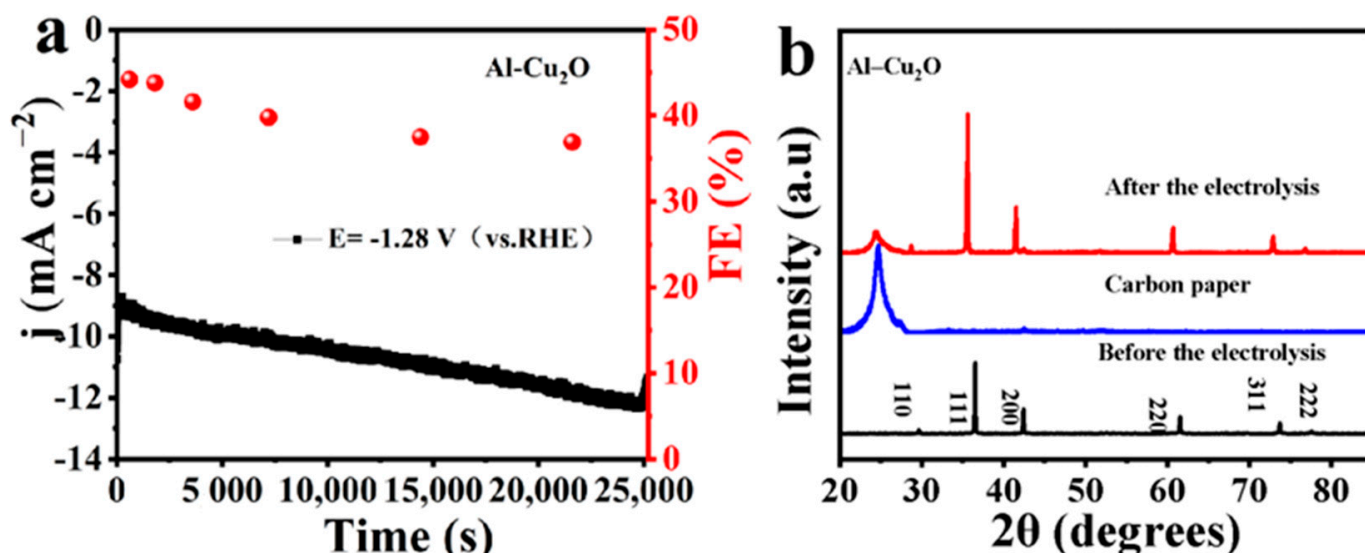


Figure 6. Al-Cu₂O catalyst in 0.1 M KHCO₃ electrolyte (a) electrochemical stability test pattern and (b) the XRD of Al-Cu₂O catalyst after long-term stability test.

2.3. DFT Computations

We used Density functional theory (DFT) to further calculate, simulate and compare the CO₂RR reaction path on the surface of Al-Cu₂O and Cu₂O catalysts to understand the path from CO₂ to C₂H₄. Figure 7 shows the spatial structure (Figure 7a) and energy distribution of Al-Cu₂O and Cu₂O. Figure 7b shows the energy distribution of ethylene production and by-product H₂ of Cu₂O and Al-Cu₂O catalysts. The Gibbs free energies of each intermediate along ethylene on Cu₂O and Al-Cu₂O catalysts *CHCOH, *CCH, *CCH, *CCH₂, *CHCH₂ (intermediates for ethylene production) and *H (intermediates to H₂) have been calculated. Because the Gibbs free energy of the Al-Cu₂O catalyst was lower than that of the Cu₂O catalyst in each reaction step, the path of ethylene production of CO₂RR was easier to occur. It can be seen that the strategy of doping Al to octahedral Cu₂O was beneficial in improving the selectivity of product C₂H₄ [41]. At the same time, the analysis of Figure 7c showed that the Al-Cu₂O catalyst with Al doping enhanced the adsorption of intermediate *H and further departed from the ideal hydrogen adsorption value (0 eV). It makes the competitive reaction of HER more disadvantageous. To further analyze the potential reason for the selective improvement of this product, the density of states (DOS) of d orbitals on Cu₂O (001) and Al-Cu₂O (001) surfaces before CHCOH adsorption was compared (Figure 7d,e). Since the electronic states near the Fermi level are mainly contributed by the d electrons of Cu atoms, it is observed that the reaction is mainly caused by the interaction between Cu and C, and the d band center of octahedron Cu₂O (001) was -2.087 eV. The -2.027 eV of the Al-Cu₂O (001) surface was closer to the Fermi level (0 eV), and the d-band shifts upward on the Abscissa, which makes the center of the d-band closer to the Fermi level and increases the density of electronic states. So, the adsorption of Cu atoms through d electrons and intermediates was facilitated, thus promoting the CO₂RR process and improving the selectivity of the catalyst for the C₂H₄ product.

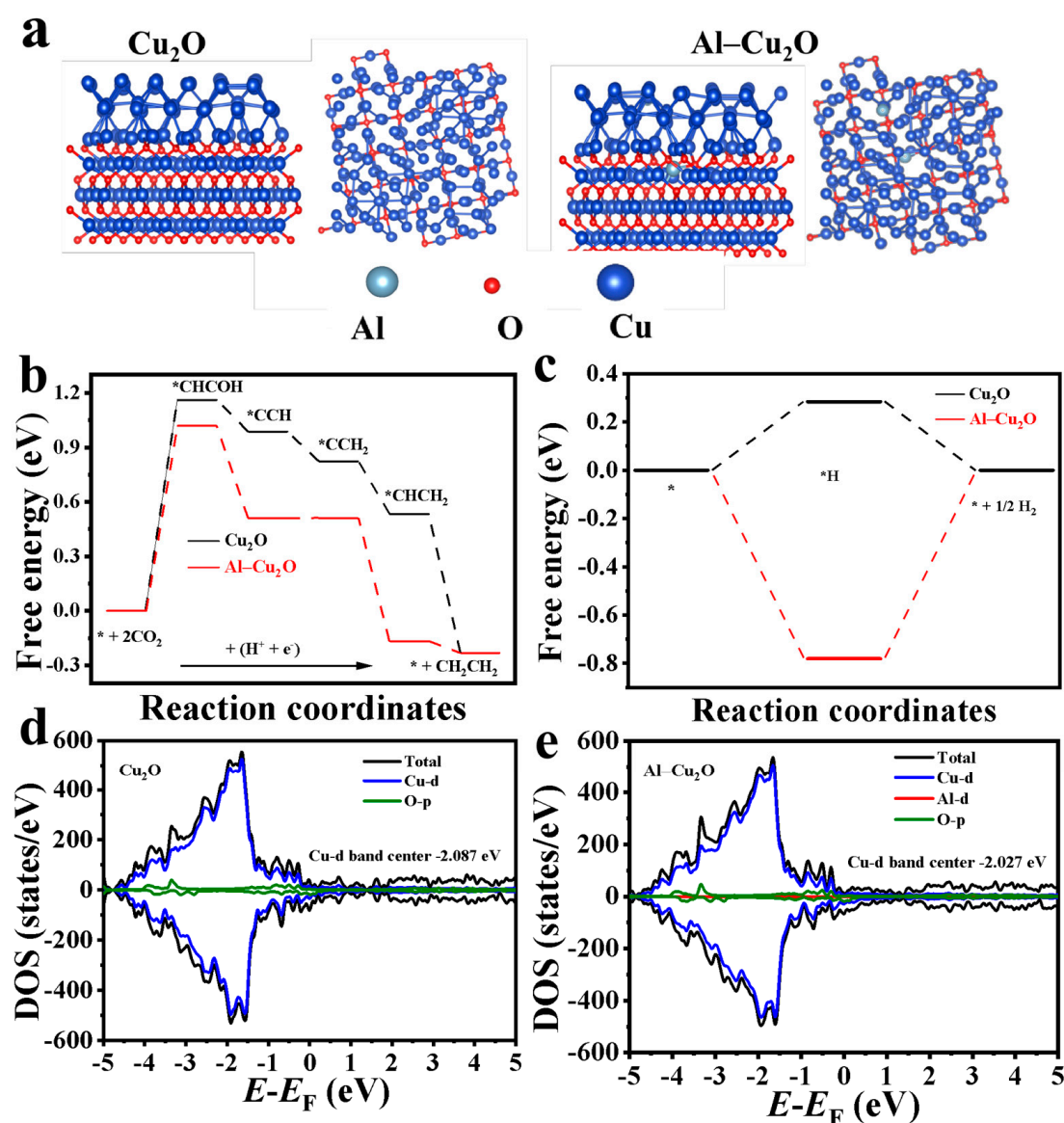


Figure 7. Free energy diagram of ethylene and hydrogen produced by CO₂RR on the surface of (a) side and top views of Cu₂O (001) and Al-Cu₂O (001) configurations, (b) Cu₂O (001) and (c) Al-Cu₂O (001) catalysts, * represents the active site; DOS of d orbitals on (d) Cu₂O (001) and (e) Al-Cu₂O (001) surfaces before *CHCOH adsorption.

3. Materials and Methods

3.1. Preparation of Al-Cu₂O Nanocrystals

The Al-Cu₂O nanocrystals were synthesized with an improved method according to the literature [42]. The specific step was as follows: 10 mL of 0.6 M NaOH aqueous solution was first added to the sample bottle. Subsequently, a certain amount of CuCl₂·2H₂O, Al(NO₃)₃·9H₂O and glucose were added to the sample bottle successively. The concentrations of CuCl₂·2H₂O, Al(NO₃)₃·9H₂O, and glucose were 0.10 M, 0.02 M, and 0.07 M, respectively. After continuous agitation for 5 min, the sample bottle was placed in a 70 °C water bath and vigorously stirred for 4 min. The precipitation obtained by centrifugal collection was rinsed with deionized water and dried under vacuum at room temperature for 12 h to obtain an Al-Cu₂O catalyst. At the same time, the effects of the amount of Al³⁺, NaOH concentration, and the sythiestic reaction time on ethylene products were also investigated in this chapter, and the optimum preparation conditions were obtained, as shown in the following Table S1.

3.2. Preparation of Al–Cu₂O Coated Carbon Paper Electrode

5 mg of the prepared catalyst was added to 25 μL of Nafion. Then, 300 μL of distilled water and 175 μL of ethanol to prepare 500 μL of reagent was added and mixed by sonication for 2 h. Subsequently, 100 μL was uniformly applied with a pipette to a carbon paper (type 060) with a total surface area of 1 cm^2 . The loading on the carbon paper was calculated to be 1 mg cm^{-2} and dried in a vacuum oven to obtain the Al–Cu₂O electrode for the next test.

3.3. Electrochemical Measurements

The electrocatalytic CO₂RR was carried out in an H-type electrolytic cell with a proton exchange membrane (Nafion 117) separation. A platinum sheet (1 cm^2) as the counter electrode and Ag/AgCl (saturated KCl) as the reference electrode, respectively. Before conducting the experimental test, CO₂ (99.999% purity) or N₂ gas was introduced into the electrolytic cell, which was saturated with 0.1 M KHCO₃ (pH = 6.8) electrolyte after approximately 30 min. In this work, all electrochemical performance was measured on the electrochemical workstation (CHI760E, Shanghai Chenhua, Shanghai, China). All electrode potentials were converted into electrode potentials relative to RHE through the Nernst equation: $E(\text{vs. RHE}) = E(\text{vs. Ag/AgCl}) + 0.0591 \times \text{pH} + 0.197 \text{ V}$. The electrochemical active surface area was tested by the cyclic voltammetry curves of the bilayer capacitance values at different scanning rates (20, 40, 60, 80, 100 and 120 mV s^{-1}). The gaseous products were collected by electrolysis of the four catalysts in a 0.1 M KHCO₃ electrolyte saturated with CO₂ for 10 min at different measurement potentials and then analyzed using gas chromatography (8890, Agilent, Santa Clara, CA, USA). The liquid products of the four catalysts were collected by electrolysis in an aqueous 0.1 M KHCO₃ solution saturated with CO₂ for 30 min at each measurement potential, followed by qualitative and quantitative analysis using ion chromatography (AS-DV, Thermo Scientific, Waltham, MA, USA).

3.4. Product Analysis

The gas products are detected by gas chromatography (GC, Agilent 8890) directly from the gas outlet. The carbonaceous gas products from the cathode chamber are analyzed by a methane reformer and flame ionization detector (FID). A thermal conductivity detector (TCD) was used to detect the eCO₂RR by-product H₂. When the current stabilizes, the gas product is detected. Quantification of the gaseous products was determined by comparison with the standard curve. The Faraday efficiency (FE) of C₂H₄, H₂ and CO was calculated as follows:

$$\text{FE} = \frac{N \times n \times v \times F}{V_m \times j} \times 100\%$$

where v is the CO₂ flow rate ($v = 20 \text{ mL min}^{-1}$), n is the total molar fraction of C₂H₄, H₂ or CO of the gas measured in the GC, N is the number of electrons required to form a molecule of H₂ or CO ($N = 2$), F is Faraday's constant (96,485 C mol^{-1}), and V_m is the molar volume of the gas at 298 K and j is current at each potential (A).

Liquid products Faraday efficiency test method: A saturated solution of electrocatalytic CO₂ was electro-catalyzed by the Coulomb method using a controlled potential, and the electrolytic reduction product was analyzed and calculated after 0.5 h. The CO₂ flow rate during electrolysis was controlled at 20 mL min^{-1} , and the liquid product was determined by ion chromatography (AS-DV, Thermo Scientific, Waltham, MA, USA). The FE of the liquid phase product was calculated as follows:

$$\text{FE} = \frac{NnF}{Q} \times 100\%$$

where N is the number of electrons transferred, n is the amount of formate in the cathode chamber, F is Faraday's constant (96,485 C mol^{-1}) and Q is the total charge passing through the electrode.

4. Conclusions

In summary, the Al-doped octahedral Cu₂O nanocrystal was successfully prepared and used as an efficient CO₂RR electrocatalyst. The Al–Cu₂O exhibited high activity and selectivity for ethylene production. The Al–Cu₂O catalyst demonstrates a high % faradaic efficiency of 44.9% at –1.23 V (vs. RHE) for C₂H₄ production. The high catalytic activity for CO₂ electrochemical reduction is due to the optimized electronic state by Al doping in octahedral Cu₂O nanocrystals. The DFT simulation suggested the C–C coupling mechanism in the electrochemical CO₂RR process. The Al–Cu₂O doped Cu₂O octahedron can significantly reduce the free energy in the coupling process of *CHCOH intermediate, promote the formation of C₂H₄, and inhibit the occurrence of HER side effect. Furthermore, our work demonstrates a simple doping strategy for preparing copper-based catalysts, which can be extended to the design and study of other highly efficient electrocatalysts.

Supplementary Materials: The following supporting information can be downloaded at: <https://www.mdpi.com/article/10.3390/ijms241612680/s1>. References [43–46] are cited in the supplementary materials.

Author Contributions: Conceptualization, J.P.; methodology, S.L. and X.S.; formal analysis, S.L., investigation, S.L., X.G. and X.S.; resources, J.P.; data curation, S.L. and X.S.; writing—original draft preparation, S.L., X.S. and J.P.; writing—review and editing, S.L., X.S. and J.P.; visualization, S.L., X.G. and X.S.; project administration, J.P.; funding acquisition, J.P. All authors have read and agreed to the published version of the manuscript.

Funding: This work was financially supported by the National Natural Science Foundation of China (No. 22262027, 22132003), Ningxia leading scientific and technological innovation talents projects (No. KJT2018002) and Ningxia Natural Science Foundation (No. 2022AAC03103).

Institutional Review Board Statement: Not applicable.

Informed Consent Statement: Not applicable.

Data Availability Statement: All data in this study can be found in public data bases and Supplementary Information, as described in the Material and Methods section (Section 3).

Conflicts of Interest: The authors declared no competing financial interest.

References

- Alli, Y.A.; Oladoye, P.O.; Ejeromedoghene, O.; Bankole, O.M.; Alimi, O.A.; Omotola, E.O.; Olanrewaju, C.A.; Philippot, K.; Adeleye, A.S.; Ogunlaja, A.S. Nanomaterials as catalysts for CO₂ transformation into value-added products: A review. *Sci. Total Environ.* **2023**, *868*, 161547. [[CrossRef](#)] [[PubMed](#)]
- Zhao, M.; Gu, Y.; Gao, W.; Cui, P.; Tang, H.; Wei, X.; Zhu, H.; Li, G.; Yan, S.; Zhang, X.; et al. Atom vacancies induced electron-rich surface of ultrathin Bi nanosheet for efficient electrochemical CO₂ reduction. *Appl. Catal. B Environ.* **2020**, *266*, 118625. [[CrossRef](#)]
- Feng, X.; Zou, H.; Zheng, R.; Wei, W.; Wang, R.; Zou, W.; Lim, G.; Hong, J.; Duan, L.; Chen, H. Bi₂O₃/BiO₂ Nanoheterojunction for Highly Efficient Electrocatalytic CO₂ Reduction to Formate. *Nano Lett.* **2022**, *22*, 1656–1664. [[CrossRef](#)] [[PubMed](#)]
- Yang, Y.; He, A.; Yang, M.; Zou, Q.; Li, H.; Liu, Z.; Tao, C.; Du, J. Selective electroreduction of CO₂ to ethanol over a highly stable catalyst derived from polyaniline/CuBi₂O₄. *Catal. Sci. Technol.* **2021**, *11*, 5908–5916. [[CrossRef](#)]
- Sakamoto, N.; Nishimura, Y.F.; Nonaka, T.; Ohashi, M.; Ishida, N.; Kitazumi, K.; Kato, Y.; Sekizawa, K.; Morikawa, T.; Arai, T. Self-assembled Cuprous Coordination Polymer as a Catalyst for CO₂ Electrochemical Reduction into C₂ Products. *ACS Catal.* **2020**, *10*, 10412–10419. [[CrossRef](#)]
- Liu, B.; Yao, X.; Zhang, Z.; Li, C.; Zhang, J.; Wang, P.; Zhao, J.; Guo, Y.; Sun, J.; Zhao, C. Synthesis of Cu₂O Nanostructures with Tunable Crystal Facets for Electrochemical CO₂ Reduction to Alcohols. *ACS Appl. Mater. Interfaces* **2021**, *13*, 39165–39177. [[CrossRef](#)]
- Zhou, X.; Shan, J.; Chen, L.; Xia, B.Y.; Ling, T.; Duan, J.; Jiao, Y.; Zheng, Y.; Qiao, S.Z. Stabilizing Cu²⁺ Ions by Solid Solutions to Promote CO₂ Electroreduction to Methane. *J. Am. Chem. Soc.* **2022**, *144*, 2079–2084. [[CrossRef](#)]
- Jiang, R.; Gao, M.; Mao, X.; Wang, D. Advancements and potentials of molten salt CO₂ capture and electrochemical transformation (MSCC-ET) process. *Curr. Opin. Electrochem.* **2019**, *17*, 38–46. [[CrossRef](#)]
- Küngas, R. Review—Electrochemical CO₂ Reduction for CO Production: Comparison of Low- and High-Temperature Electrolysis Technologies. *J. Electrochem. Soc.* **2020**, *167*, 044508. [[CrossRef](#)]
- Lacarbonara, G.; Chini, S.; Ratso, S.; Kruusenberg, I.; Arbizzani, C. A MnOx–graphitic carbon composite from CO₂ for sustainable Li-ion battery anodes. *Mater. Adv.* **2022**, *3*, 7087–7097. [[CrossRef](#)]

11. Rimmel, A.-L.; Ratso, S.; Divitini, G.; Danilson, M.; Mikli, V.; Uibu, M.; Aruväli, J.; Kruusenberg, I. Nickel and Nitrogen-Doped Bifunctional ORR and HER Electrocatalysts Derived from CO₂. *ACS Sustain. Chem. Eng.* **2021**, *10*, 134–145. [[CrossRef](#)]
12. Dong, W.; Zhang, N.; Li, S.; Min, S.; Peng, J.; Liu, W.; Zhan, D.; Bai, H. A Mn single atom catalyst with Mn–N₂O₂ sites integrated into carbon nanosheets for efficient electrocatalytic CO₂ reduction. *J. Mater. Chem. A* **2022**, *10*, 10892–10901. [[CrossRef](#)]
13. Clark, E.L.; Ringe, S.; Tang, M.; Walton, A.; Hahn, C.; Jaramillo, T.F.; Chan, K.; Bell, A.T. Influence of Atomic Surface Structure on the Activity of Ag for the Electrochemical Reduction of CO₂ to CO. *ACS Catal.* **2019**, *9*, 4006–4014. [[CrossRef](#)]
14. Wang, Q.; Liu, K.; Hu, K.; Cai, C.; Li, H.; Li, H.; Herran, M.; Lu, Y.-R.; Chan, T.-S.; Ma, C. Attenuating metal-substrate conjugation in atomically dispersed nickel catalysts for electroreduction of CO₂ to CO. *Nat. Commun.* **2022**, *13*, 6082. [[CrossRef](#)] [[PubMed](#)]
15. Duan, Y.X.; Zhou, Y.T.; Yu, Z.; Liu, D.X.; Wen, Z.; Yan, J.M.; Jiang, Q. Boosting production of HCOOH from CO₂ electroreduction via Bi/CeO_x. *Angew. Chem. Int. Ed.* **2021**, *60*, 8798–8802. [[CrossRef](#)]
16. Koh, J.H.; Won, D.H.; Eom, T.; Kim, N.-K.; Jung, K.D.; Kim, H.; Hwang, Y.J.; Min, B.K. Facile CO₂ electro-reduction to formate via oxygen bidentate intermediate stabilized by high-index planes of Bi dendrite catalyst. *ACS Catal.* **2017**, *7*, 5071–5077. [[CrossRef](#)]
17. Li, D.; Huang, L.; Tian, Y.; Liu, T.; Zhen, L.; Feng, Y. Facile synthesis of porous Cu-Sn alloy electrode with prior selectivity of formate in a wide potential range for CO₂ electrochemical reduction. *Appl. Catal. B Environ.* **2021**, *292*, 120119. [[CrossRef](#)]
18. Grace, A.N.; Choi, S.Y.; Vinoba, M.; Bhagiyalakshmi, M.; Chu, D.H.; Yoon, Y.; Nam, S.C.; Jeong, S.K. Electrochemical reduction of carbon dioxide at low overpotential on a polyaniline/Cu₂O nanocomposite based electrode. *Appl. Energy* **2014**, *120*, 85–94. [[CrossRef](#)]
19. Boutin, E.; Wang, M.; Lin, J.C.; Mesnage, M.; Mendoza, D.; Lassalle-Kaiser, B.; Hahn, C.; Jaramillo, T.F.; Robert, M. Aqueous electrochemical reduction of carbon dioxide and carbon monoxide into methanol with cobalt phthalocyanine. *Angew. Chem. Int. Ed.* **2019**, *58*, 16172–16176. [[CrossRef](#)]
20. Ren, D.; Deng, Y.; Handoko, A.D.; Chen, C.S.; Malkhandi, S.; Yeo, B.S. Selective electrochemical reduction of carbon dioxide to ethylene and ethanol on copper (I) oxide catalysts. *ACS Catal.* **2015**, *5*, 2814–2821. [[CrossRef](#)]
21. Yuan, J.; Yang, M.-P.; Zhi, W.-Y.; Wang, H.; Wang, H.; Lu, J.-X. Efficient electrochemical reduction of CO₂ to ethanol on Cu nanoparticles decorated on N-doped graphene oxide catalysts. *J. CO₂ Util.* **2019**, *33*, 452–460. [[CrossRef](#)]
22. Iyengar, P.; Huang, J.; De Gregorio, G.L.; Gadiyar, C.; Buonsanti, R. Size dependent selectivity of Cu nano-octahedra catalysts for the electrochemical reduction of CO₂ to CH₄. *Chem. Commun.* **2019**, *55*, 8796–8799. [[CrossRef](#)]
23. Chu, S.; Kang, C.; Park, W.; Han, Y.; Hong, S.; Hao, L.; Zhang, H.; Lo, T.W.B.; Robertson, A.W.; Jung, Y. Single atom and defect engineering of CuO for efficient electrochemical reduction of CO₂ to C₂H₄. *SmartMat* **2022**, *3*, 194–205. [[CrossRef](#)]
24. Luo, H.; Li, B.; Ma, J.G.; Cheng, P. Surface Modification of Nano-Cu₂O for Controlling CO₂ Electrochemical Reduction to Ethylene and Syngas. *Angew. Chem. Int. Ed.* **2022**, *61*, e202116736. [[CrossRef](#)]
25. Tan, X.; Yu, C.; Zhao, C.; Huang, H.; Yao, X.; Han, X.; Guo, W.; Cui, S.; Huang, H.; Qiu, J. Interfaces, Restructuring of Cu₂O to Cu₂O@Cu-metal-organic frameworks for selective electrochemical reduction of CO₂. *ACS Appl. Mater. Interfaces* **2019**, *11*, 9904–9910. [[CrossRef](#)]
26. Cao, S.; Chen, H.; Han, T.; Zhao, C.; Peng, L. Rose-like Cu₂O nanoflowers via hydrothermal synthesis and their gas sensing properties. *Mater. Lett.* **2016**, *180*, 135–139. [[CrossRef](#)]
27. Gao, Y.; Wu, Q.; Liang, X.; Wang, Z.; Zheng, Z.; Wang, P.; Liu, Y.; Dai, Y.; Whangbo, M.H.; Huang, B. Cu₂O Nanoparticles with Both 100 and 111 Facets for Enhancing the Selectivity and Activity of CO₂ Electroreduction to Ethylene. *Adv. Sci.* **2020**, *7*, 1902820. [[CrossRef](#)]
28. Fu, W.; Liu, Z.; Wang, T.; Liang, J.; Duan, S.; Xie, L.; Han, J.; Li, Q. Engineering, Promoting C²⁺ production from electrochemical CO₂ reduction on shape-controlled cuprous oxide nanocrystals with high-index facets. *ACS Sustain. Chem. Eng.* **2020**, *8*, 15223–15229. [[CrossRef](#)]
29. Luo, T.; Liu, K.; Fu, J.; Chen, S.; Li, H.; Hu, J.; Liu, M. Tandem catalysis on adjacent active motifs of copper grain boundary for efficient CO₂ electroreduction toward C₂ products. *J. Energy Chem.* **2022**, *70*, 219–223. [[CrossRef](#)]
30. Wang, Y.; Lou, Z.; Niu, W.; Ye, Z.; Zhu, L. Optimization of photoelectrochemical performance in Pt-modified p-Cu₂O/n-Cu₂O nanocomposite. *Nanotechnology* **2018**, *29*, 145402. [[CrossRef](#)]
31. Feng, Y.; Li, Z.; Liu, H.; Dong, C.; Wang, J.; Kulinich, S.A.; Du, X. Laser-prepared CuZn alloy catalyst for selective electrochemical reduction of CO₂ to ethylene. *Langmuir* **2018**, *34*, 13544–13549. [[CrossRef](#)]
32. Chen, C.; Sun, X.; Yan, X.; Wu, Y.; Liu, M.; Liu, S.; Zhao, Z.; Han, B. A strategy to control the grain boundary density and Cu⁺/Cu⁰ ratio of Cu-based catalysts for efficient electroreduction of CO₂ to C₂ products. *Green Chem.* **2020**, *22*, 1572–1576. [[CrossRef](#)]
33. Shang, L.; Lv, X.; Shen, H.; Shao, Z.; Zheng, G. Selective carbon dioxide electroreduction to ethylene and ethanol by core-shell copper/cuprous oxide. *J. Colloid Interface Sci.* **2019**, *552*, 426–431. [[CrossRef](#)] [[PubMed](#)]
34. Ning, H.; Wang, X.; Wang, W.; Mao, Q.; Yang, Z.; Zhao, Q.; Song, Y.; Wu, M. Cubic Cu₂O on nitrogen-doped carbon shells for electrocatalytic CO₂ reduction to C₂H₄. *Carbon* **2019**, *146*, 218–223. [[CrossRef](#)]
35. Chang, X.; Wang, T.; Zhao, Z.J.; Yang, P.; Greeley, J.; Mu, R.; Zhang, G.; Gong, Z.; Luo, Z.; Chen, J. Tuning Cu/Cu₂O interfaces for the reduction of carbon dioxide to methanol in aqueous solutions. *Angew. Chem. Int. Ed.* **2018**, *57*, 15415–15419. [[CrossRef](#)]
36. Qiu, Y.-L.; Zhong, H.-X.; Zhang, T.-T.; Xu, W.-B.; Li, X.-F.; Zhang, H.-M. Copper Electrode Fabricated via Pulse Electrodeposition: Toward High Methane Selectivity and Activity for CO₂ Electroreduction. *ACS Catal.* **2017**, *7*, 6302–6310. [[CrossRef](#)]

37. Zheng, Y.; Zhang, L.; Guan, J.; Qian, S.; Zhang, Z.; Ngaw, C.K.; Wan, S.; Wang, S.; Lin, J.; Wang, Y.; et al. Engineering, Controlled synthesis of Cu⁰/Cu₂O for efficient photothermal catalytic conversion of CO₂ and H₂O. *ACS Sustain. Chem. Eng.* **2021**, *9*, 1754–1761. [[CrossRef](#)]
38. Wang, S.; Kou, T.; Varley, J.B.; Akhade, S.A.; Weitzner, S.E.; Baker, S.E.; Duoss, E.B.; Li, Y. Cu₂O/CuS nanocomposites show excellent selectivity and stability for formate generation via electrochemical reduction of carbon dioxide. *ACS Mater. Lett.* **2020**, *3*, 100–109. [[CrossRef](#)]
39. Lv, X.-W.; Liu, Y.; Hao, R.; Tian, W.; Yuan, Z.-Y. Urchin-like Al-doped Co₃O₄ nanospheres rich in surface oxygen vacancies enable efficient ammonia electrosynthesis. *ACS Appl. Mater. Interfaces* **2020**, *12*, 17502–17508. [[CrossRef](#)]
40. Sun, B.; Dai, M.; Cai, S.; Cheng, H.; Song, K.; Yu, Y.; Hu, H. Challenges and strategies towards copper-based catalysts for enhanced electrochemical CO₂ reduction to multi-carbon products. *Fuel* **2023**, *332*, 126114. [[CrossRef](#)]
41. Li, Y.C.; Wang, Z.; Yuan, T.; Nam, D.-H.; Luo, M.; Wicks, J.; Chen, B.; Li, J.; Li, F.; de Arquer, F.P.G.; et al. Binding Site Diversity Promotes CO₂ Electroreduction to Ethanol. *J. Am. Chem. Soc.* **2019**, *141*, 8584–8591. [[CrossRef](#)]
42. Yang, R.; Wu, Z.; Tang, D.; Xing, Y.; Ren, Y.; Li, F.; Li, X. Synthesis of Cu₂O crystals with negative surface curvature at various positions via Al³⁺ ions inducing. *Mater. Lett.* **2014**, *117*, 211–213. [[CrossRef](#)]
43. Kresse, G.; Furthmüller, J.J. Efficient iterative schemes for ab initio total-energy calculations using a plane-wave basis set. *Phys. Rev. B* **1996**, *54*, 11169. [[CrossRef](#)] [[PubMed](#)]
44. Perdew, J.P.; Burke, K.; Ernzerhof, M.J. Generalized gradient approximation made simple. *Phys. Rev. Lett.* **1996**, *77*, 3865. [[CrossRef](#)]
45. Hammer, B.; Hansen, L.B.; Nørskov, J.K. Improved adsorption energetics within density-functional theory using revised Perdew-Burke-Ernzerhof functionals. *Phys. Rev. B* **1999**, *59*, 7413. [[CrossRef](#)]
46. Grimme, S.J. Semiempirical GGA-type density functional constructed with a long-range dispersion correction. *J. Comput. Chem.* **2006**, *27*, 1787–1799. [[CrossRef](#)]

Disclaimer/Publisher's Note: The statements, opinions and data contained in all publications are solely those of the individual author(s) and contributor(s) and not of MDPI and/or the editor(s). MDPI and/or the editor(s) disclaim responsibility for any injury to people or property resulting from any ideas, methods, instructions or products referred to in the content.